 CMES, vol.115, no.3, pp.387-409, 2018

Theory and Calculation of the *J*-Integral for Coupled Chemo-Mechanical Fracture Mechanics

Wei Wei[1], Qingsheng Yang[2,*], Xia Liu[2], Xiaoqiao He[3,*] and Kim-Meow Liew[3]

Abstract: In this paper, by introducing a chemical field, the *J*-integral formulation is presented for the chemo-mechanical coupled medium based on the laws of thermodynamics. A finite element implementation of the *J*-integral was performed to study the mode I chemo-mechanical coupled fracture problem. For derivation of the coupled *J*-integral, the equivalent domain integral (EDI) method was applied to obtain the mode I *J*-integral, with expression of the area integrals based on constitutive relationships of a linear elastic small deformation for chemo-mechanical coupling, instead of the finite deformation problem. A finite element procedure is developed to compute the mode I *J*-integral, and numerical simulation of the *y*-direction stress field is studied by a subroutine UEL (User defined element) developed in ABAQUS software. Accuracy of the numerical results obtained using the mode I *J*-integral was verified by comparing them to a well-established model based on linear elastic fracture mechanics (LEFM). Furthermore, a numerical example was presented to illustrate path-independence of the formulated *J*-integral for a chemo-mechanical coupled specimen under different boundary conditions, showing a high accuracy and reliability of the present method. The variation laws of *J*-integral and the *y*-direction stress field with external chemical, mechanical loading and time are revealed. The *J*-integral value increases with larger external concentration loading in the same integral domain. The extent of diffusion is much greater with larger concentration, which leads to a stronger coupling effect due to the chemical field. This work provides new insights into the fracture mechanics for the chemo-mechanical coupled medium.

Keywords: Chemo-mechanical coupling, fracture, *J*-integral, equivalent domain integral (EDI) method, finite element method.

1 Introduction

A number of media are known to exhibit chemo-mechanical coupling behavior including polymer colloids, hydrogels, biological tissues, and lithium ion batteries. Hydrogels are composed of a water-swollen and cross-linked polymeric network and are capable of

[1] School of Civil Engineering, Hebei University of Engineering, Handan 056038, China.

[2] Department of Engineering Mechanics, Beijing University of Technology, Beijing 100124, China.

[3] Department of Civil and Architectural Engineering, City University of Hong Kong, Tat Chee Avenue, Kowloon, Hong Kong.

* Corresponding Author: Qingsheng Yang. Email: qsyang@bjut.edu.cn; Xiaoqiao He. Email: bcxqhe@cityu.edu.hk.

reversible deformation when subjected to mechanical forces and/or environmental stimuli (e.g. temperature, pH, humidity). To date, several functional components have been designed and manufactured using chemo-mechanical coupled characteristics in a variety of applications, ranging from artificial organs [Shao, Jia, Cao et al. (2017)], drug delivery [Javanbakht and Namazi (2018)], actuators and sensors [Cheng, Ren, Yang et al. (2018); Deng, Bellmann, Fu et al. (2018)], oil packaging [Mahinroosta, Farsangi, Allahverdi et al. (2018)], contact lenses [Alvarez-Rivera, Concheiro and Alvarez-Lorenzo (2018)], and wound dressings [Khorasani, Joorabloo, Moghaddam et al. (2018)].

Cracking is a critical concern in designing chemo-mechanical coupled hydrogel components. Cracks may lead to poor mechanical stability, and eventually cause structural failure of the entire system. Moreover, in biological applications involving cell encapsulation, cracks may lead to involuntary cell release or possible cell death. Hydrogels have been used as microfluidic valves for lab-on-a-chip systems, which require appropriate measures to ensure that cracks do not lead to liquid leakage causing failure of the device. In recent years, a large number of fracture phenomena have been observed in intelligent hydrogels during experiments [Cai, Hu, Zhao et al. (2010); Sun, Zhao, Illeperuma et al. (2012); Pizzocolo, Huyghe and Ito (2013)]. Optical microscope observations of synthetic hydrogels during and after tensile testing experiments have demonstrated medium-sized fracture processes. For these reasons, the fracture behavior of chemo-mechanical coupled media has become a subject of rising scientific interest.

Despite the emergence of chemo-mechanical coupling as an important research field, there is limited literature analyzing fracture problems occurring in such systems. The fracture problems of chemo-mechanical coupled media have not yet to be fully elucidated. Moreover, although most chemo-mechanical coupled media exhibit liquid-like behavior they are often considered to be perfectly elastic and functional solids. Analysis using the *J*-integral has been widely performed to study the fracture problems of other multi-field coupling phenomena. Fracture mechanics problems in thermo-mechanical, electro-mechanical and thermo-electro-mechanical coupled media have long always been gaining extensive interests in electromechanical devices, microelectromechanical systems and smart composite materials. In order to assess fracture properties of these media, exhaustive theoretical, numerical and experimental investigations on the *J*-integral have been performed in the past few decades. Modified forms of *J*-integral were presented to extract the magnitude of stress intensity factors from finite element solutions for homogeneous materials subjected to thermal stresses [Wilson and Yu (1979); Li (1993)]. The viability of the domain integral method and corresponding finite element formulation were demonstrated for calculating the pointwise energy release rate based on a path-independent *J*-integral under thermo-mechanical loadings [Li, Shih and Needleman (1985); Shih, Moran and Nakamura (1986)]. The EDI approach and the numerical implementation for thermo-mechanical fracture analysis were described thoroughly in homogeneous materials [Nikishkov and Atluri (1987); Raju and Shivakumar (1990)]. The path-independent J and J_k^* integrals were applied for evaluating numerically stress intensity factors (SIFs) and fracture parameters by means of the EDI method subjected to thermo-mechanical loading in functionally graded materials (FGMs) [Kim and Paulino (2002), Kim and Paulino (2003); Walters, Paulino and Dodds (2004)]. The generalized

J_k-integral and SIFs subjected to mode I and mixed-mode crack problems for FGMs were calculated by using the EDI method [Yildirim (2006); Dag (2007)]. A thermo-electro-mechanical *J*-integral formulation by using the laws of thermodynamics was derived for computing coupled crack problems in thermopiezoelectric structures [Kuna (2006); Ricoeur and Kuna (2008)]. A modified domain-independent interaction integral based on the *J*-integral combined with XFEM method was presented to investigate the influences of material continuity on the SIFs, TSIFs and EDIF of nonhomogeneous piezoelectric materials [Yu, Wu, Guo et al. (2012); Guo, Guo, Yu et al. (2014)]. The *J*-integral method can give highest accuracy compared to other calculating methods for evaluating the SIFs in two-dimensional piezoelectric solids [Lei, Wang, Zhang et al. (2014)]. A thermodynamic formulation of *J*-integral considering residual stress and thermal stress was presented to prove the independence of the *J*-integral for a welded component [Park, Choi, Kim et al. (2015)]. Ding et al. [Ding and Liu (2018)] developed a multi-layered model for heat conduction analysis of a thermoelectric material strip (TEMs) with a Griffith crack, and studied the effect of strip width on the electric flux intensity factor and thermal flux intensity factor.

Among numerous existing studies on the fracture behavior under combined chemo-mechanical loading, few also have utilized the conventional *J*-integral to analyze crack problems. Furthermore, unlike the aforementioned systems, the poroelastic property of chemo-mechanical coupled media cannot be ignored due to the influence of solvent diffusion together with the coupling effects of chemical and stress fields on the fracture processes. The effects of solvent diffusion on fracture were studied within the general framework of poroelasticity [Rice and Cleary (1976)]. Bonn et al. [Bonn, Kellay, Prochnow et al. (1998)] discovered the phenomena of delayed fracture due to the solvent diffusion in polymer gels, which is ascribed to the time effect of solvent migration caused by viscoelastic creep and transient energy release rates [Wang and Hong (2012)]. A general form of energy release rate was derived and rewritten as a simplified path independent integral for hygrothermal elastic coupling fracture problems [Yang, Wang and Chen (2006)]. A *J*-integral formulation was developed for analyzing the coupled mechano-diffusional driving forces for fracture in Li-ion batteries through a fully-coupled finite deformation theory [Gao and Zhou (2013)]. Hui et al. [Hui, Long and Ning (2013)] studied the transient stress and pore pressure field near the static Mode I crack tip in poroelastic solids subjected to transient loading. An electro-chemo-mechanical *J*-integral under equilibrium conditions was constructed for demonstrating the path-independent nature of the chemo-mechanical *J*-integral in solid [Haftbaradaran and Qu (2014)]. A thermodynamically consistent method was presented for calculating the transient energy release rate based on a modified path-independent *J*-integral, considering the effect of solvent diffusion on crack growth in hydrogels [Bouklas, Landis and Huang (2015)]. The energy release rate was derived within the linearized, small-strain scope for the poroelastic nature of polymer gels [Noselli, Lucantonio, Mcmeeking et al. (2016)]. Tang et al. [Tang, Li, Vlassak et al. (2017)] observed three types of fracture behavior in the hydrogel: fast fracture, delayed fracture, and fatigue fracture, and concluded the concentration of water and the amplitude of load can significantly affect the fracture behavior. Zhang et al. [Zhang, Qu and Rice (2017)] constructed the *J*- and *L*-integrals which are two types of path-independent integrals in equilibrium electro-chemo-elasticity

in the solid, representing the energy release when a cavity translates and rotates, respectively. Böger et al. [Böger, Keip and Miehe (2017)] proposed a diffusion-deformation-fracture theory with a diffuse-crack approximation based on a phase-field/damage fracture theory, and presented a variational framework together with a numerical implementation in a finite element program. Yu et al. [Yu, Wang, Chen et al. (2017); Yu, Chen, Wang et al. (2018)] obtained several path-independent integrals, including the *J*-, *L*- and *M*-integrals of the dissipative chemo-electro-mechanical processes, and addressed the chemical reactions by the path-independence *J*-integral and verified the relation of the *J*-integral and *L*-integral with the energy release rate. Ma et al. [Ma and Yang (2018)] developed a micromechanics model incorporating fluid pressure, which can be used to determine the stress and strain fields at the tip of fluid-filled cracks in porous materials. Mao et al. [Mao and Anand (2018)] formulated a theory which accounts for the coupled effects of fluid diffusion, large deformations, damage, and also the gradient effects of damage for fracture of polymeric gels, and proposed the particular constitutive equations for fracture of a gel. Yang et al. [Yang and Lin (2018)] analyzed the concurrent deformation of the solid network and migration of interstitial fluid by using *J*-integral around a crack tip in a poroviscoelastic medium under mode-I condition.

In this paper, the combined effects of volumetric swelling and stress under chemo-mechanical coupling were addressed. The main objective of this work was to derive the *J*-integral formulation for a mode I crack under chemo-mechanical coupling and develop a finite element procedure by means of the equivalent domain integral (EDI) method for fracture analysis in the chemo-mechanical coupled medium.

The *J*-integral in the most of previous works were derived from the energy release rate [Gao and Zhou (2013); Bouklas, Landis and Huang (2015); Noselli, Lucantonio, Mcmeeking et al. (2016)]. In comparison to these studies, although the final form of the *J*-integral is similar, the theoretical derivation process of the *J*-integral formulation is a completely unique way in the paper. The chemo-mechanical coupled *J*-integral formula is deduced using the first law of thermodynamics that takes into account chemical energy instead of the usage of the energy release rate. In addition, in this paper，by using a unique chemo-mechanical coupled constitutive relation derived by Wei et al. [Wei and Yang (2016)], the mode I *J*-integral formula that contains the chemo-mechanical coupled constitutive relations can be deduced. Moreover, other people's theories are based on the large deformation theory, but this paper is based on the assumption of the linear-elastic small deformation theory for the chemo-mechanical coupled medium. The mode I *J*-integral value of a crack is calculated by the *J*-integral calculation program developed, by which the variation law of *J*-integral is analyzed with different parameters. In the meantime, the *y*-direction stress field of a crack is numerically simulated with ABAQUS software including subroutine UEL (User defined element) developed by Wei et al. [Wei and Yang (2016)]. These processes are completely different from Gao et al. [Gao and Zhou (2013)], Bouklas et al. [Bouklas, Landis and Huang (2015)], and Noselli et al. [Noselli, Lucantonio, Mcmeeking et al. (2016)].

The paper is organized as follows. In Section 2, the *J*-integral formulation for a mode I fracture is deduced based on the laws of thermodynamics for chemo-mechanical coupling. Section 3 presents an equivalent domain form of mode I chemo-mechanical coupled

J-integral derived by means of EDI method around the crack tip. Section 4 comprises the finite element implementation of the *J*-integral for a mode I crack under chemo-mechanical coupling. Section 5 presents numerical examples, which were performed and interpreted to assess the *y*-direction stress field and *J*-integral characteristic around the crack tip. Finally, some concluding remarks are given in Section 6.

2 *J*-integral formulation for chemo-mechanical coupling problem

According to the first law of thermodynamics, considering an infinitesimal volume d*V*, the local energy balance [Ricoeur and Kuna (2008)] of a chemo-mechanical coupled medium is given by

$$\delta U = \delta Q + \delta W^{rev} + \delta \psi \tag{1}$$

where δU is the change in internal energy, δQ is the exchange of heat, δW^{rev} is the reversible work, and $\delta \psi$ is the irreversible dissipative work.

If there exists a dislocation or a defect (crack) within the finite volume *V*, the total dissipative work can be characterized as

$$\int_V \delta \psi dV = J_k \delta z_k \tag{2}$$

where J_k is a generalized force acting on the defect, and δz_k is the irreversible displacement.

Based on the energy representation derived [Ricoeur and Kuna (2009)], ignoring the role of electrostatic field, and introducing the effects of a chemical field in conjunction with the Legendre transformation, the relationship between the internal energy density function $U(\varepsilon_{ij}, \eta, \mu)$ and the free energy density function $W(\varepsilon_{ij}, T, c)$ can be expressed as

$$U = W - \mu c - \eta T \tag{3}$$

where ε_{ij} is the strain, η is the entropy, μ is the chemical potential, and *T* and *c* are the temperature and solvent concentration, respectively. Based on Eq. (3), the change in internal energy is

$$\delta U = \delta W - \mu \delta c - c \delta \mu - \eta \delta T - T \delta \eta \tag{4}$$

If all dissipative processes have been included in $\delta \psi$, reversible work and heat are denoted by $\delta W^{rev} = \sigma_{ij} \delta \varepsilon_{ij} - c \delta \mu$ and $\delta Q = -T \delta \eta$, respectively. Consequently, Eq. (1) becomes

$$\delta \psi = \delta W - \sigma_{ij} \delta \varepsilon_{ij} - \mu \delta c - \eta \delta T \tag{5}$$

Substituting Eq. (5) into Eq. (2) yields the global energy balance for *V*

$$J_k \delta z_k = \int_V \delta \psi dV = \int_V \left(\delta W - \sigma_{ij} \delta \varepsilon_{ij} - \mu \delta c - \eta \delta T \right) dV \tag{6}$$

The virtual displacement δz_k can be adopted to incorporate changes in the state variables, such that

$$\int_V \delta W dV = \delta \overline{W} = \frac{d\overline{W}}{dx_k}\delta z_k = \int_V \left(W\delta_{kj}\right)_{,j} dV\delta z_k \tag{7}$$

Similarly, it can be concluded that $\mu\delta c = \mu c_{,k}\delta z_k$, and $\sigma_{ij}\delta\varepsilon_{ij} = \left(\sigma_{ij}u_{i,k}\right)_{,j}\delta z_k$. It should be noted that the volume force is omitted in Eq. (9), i.e. $\sigma_{ij,j} = 0$. Assuming the internal temperature of the system remains constant and substituting Eq. (7) into Eq. (6), lead to

$$J_k = \int_V \left[\left(W\delta_{kj}\right)_{,j} - \left(\sigma_{ij}u_{i,k}\right)_{,j} - \mu c_{,k}\right] dV \tag{8}$$

where δ_{kj} denotes the Kronecker delta. Applying the divergence theorem to a domain surrounded by Σ with unit outward normal n_j, gives

$$J_k = \oint_\Sigma \left(Wn_k - \sigma_{ij}n_j u_{i,k}\right) dA - \int_V \left(\mu c_{,k}\right) dV \qquad (i, j, k = 1, 2, 3) \tag{9}$$

The physical meaning of J_k is the generalized force applying on the crack tip of the elastic chemo-mechanical coupling medium. A sharp crack subjected to chemo-mechanical coupling is shown in Fig. 1.

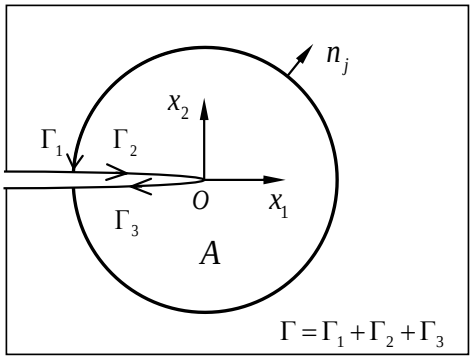

Figure 1: Schematic diagram of a sharp crack

Considering the two-dimensional plane strain state shown in Fig. 1, the chemo-mechanical coupled *J*-integral formulated can be represented as

$$J_k = \oint_\Gamma \left(Wn_k - \sigma_{ij}n_j u_{i,k}\right) \mathrm{d}\Gamma - \int_A \left(\mu c_{,k}\right) \mathrm{d}A \quad (i, j, k = 1, 2) \tag{10}$$

where A is the area surrounded by a closed contour Γ comprising $\Gamma_1, \Gamma_2, \Gamma_3$.

When k = 1, the chemo-mechanical coupled mode I J-integral formulated can be expressed as

$$J_1 = \oint_\Gamma \left(Wn_1 - \sigma_{ij}n_j u_{i,1}\right) d\Gamma - \int_A \left(\mu c_{,1}\right) dA \qquad (i, j = 1, 2) \tag{11}$$

When k = 2, J_K integral can be written as

$$J_2 = \oint_\Gamma \left(Wn_2 - \sigma_{ij}n_j u_{i,2}\right) d\Gamma - \int_A \left(\mu c_{,2}\right) dA \qquad (i, j = 1, 2) \tag{12}$$

The Eq. (12) can be used to solve the mixed-mode fracture problem under chemo-

mechanical coupling.

If the cracks are straight on the surfaces of Γ_2 and Γ_3, a value n_1=0 is achieved. Taking into account the traction-free condition on the crack surfaces (Fig. 1), it can be obtained $\sigma_{ij}n_j = T_i = 0$, so the *J*-integral can be denoted as

$$J_1 = \int_{\Gamma_1}\left(Wn_1 - \sigma_{ij}n_j u_{i,1}\right)d\Gamma - \int_A \left(\mu c_{,1}\right)dA \qquad (i,j=1,2) \tag{13}$$

This form of the *J*-integral is similar to those reported in the literatures, in which the *J*-integral in the most of previous works were derived from the energy release rate [Gao and Zhou (2013); Bouklas, Landis and Huang (2015); Noselli, Lucantonio, Mcmeeking et al. (2016)]. However, the theoretical derivation process of the *J*-integral formulation is a completely unique way in the paper. The chemo-mechanical coupled *J*-integral formula is derived using the first law of thermodynamics which considers chemical energy rather than the usage of the energy release rate. Furthermore, based on mechanical equilibrium and mass conservation, it can be deduced that the chemo-mechanical coupled *J*-integral is conserved and necessarily zero for these conditions. For a domain containing a crack tip (Fig. 1), the chemo-mechanical coupled *J*-integral is path-independent, and an area integral must be considered to maintain path-independence.

3 Equivalent domain integral method for coupled *J*-integral with a mode I crack

The EDI method is widely used in numerical calculations. Using the EDI method, the *J*-integral can be converted to an area integral, replacing the integral loop by a limited region near the crack tip to effectively evaluate the *J*-integral value [Moura and Shih (1987); Shivakumar and Raju (1992)].

A crack in a homogeneous medium, which is subjected to a chemo-mechanical coupling effect, is depicted in Fig. 2.

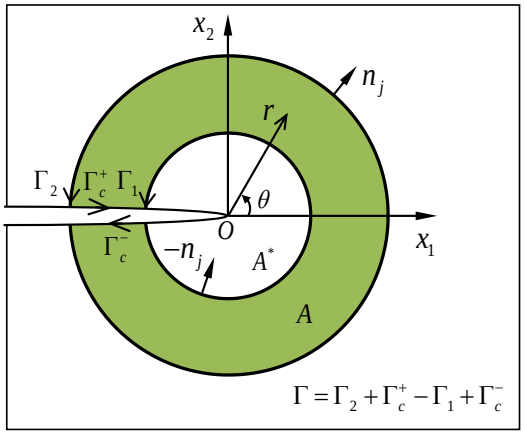

Figure 2: A closed contour Γ around the crack tip

An arbitrary closed curve Γ_1 starts from the lower crack and terminates on the upper one (counterclockwise direction). Again, n_j represents the unit outward normal. Supposing A^* is the area surrounded by Γ_1 in Fig. 2, Eq. (13) can be expressed as

$$J_1 = \int_{\Gamma_1} \left(W n_1 - \sigma_{ij} n_j u_{i,1} \right) d\Gamma - \int_{A^*} \left(\mu c_{,1} \right) dA \qquad (i, j = 1,2) \tag{14}$$

To carry out the numerical calculations in this section, the line integral in Eq. (14) can be converted to a domain integral using the EDI method. If we consider a positively-oriented closed contour curve Γ bounding the annular area A around the crack tip, as shown in Fig. 2, Γ is piecewise smooth and can be represented by $\Gamma = \Gamma_2 + \Gamma_c^+ - \Gamma_1 + \Gamma_c^-$. The method originally proposed by Shih et al. [Shih, Moran and Nakamura (1986)] can be adopted to convert the contour integral into a domain integral in order to compute the J-integral in the present study.

The chemo-mechanical coupled medium is assumed to be an elastic homogeneous medium. Therefore, using the relationship for infinitesimal displacements $\varepsilon_{ij} = \left(u_{i,j} + u_{j,i} \right) / 2 \ \ (i, j = 1,2)$ and $\partial W / \partial \varepsilon_{ij} = \sigma_{ij} \ \ (i, j = 1,2)$, for both plane stress and plane strain states, we have

$$W_{,1} = \frac{\partial W}{\partial \varepsilon_{ij}} \frac{\partial \varepsilon_{ij}}{\partial x_1} + \frac{\partial W}{\partial c} \frac{\partial c}{\partial x_1} = \sigma_{ij} u_{i,1j} + \left(W_{,1} \right)_{\exp} \qquad (i, j = 1,2) \tag{15}$$

Supposing the first component of the unit outward normal $n_1 = 0$, together with q=1 in area A*, the mode I J-integral can be written as

$$J_1 = \int_A \left(\sigma_{ij} u_{i,1} - W \delta_{1j} \right) q_{,j} dA - \int_A \left[\left(W_{,1} \right)_{\exp} \right] q dA - \int_{A^*} \left(\mu c_{,1} \right) q dA \qquad (i, j = 1,2) \tag{16}$$

where q is a sufficiently piecewise smooth arbitrary weight function in A in which $q_{\Gamma_1} = 1$ on the inner curve Γ_1 and $q_{\Gamma_2} = 0$ on the outer curve Γ_2. In general, q is known as the plateau type function.

4 Finite element implementation for coupled *J*-integral with mode I crack

Linear constitutive equations of chemo-mechanical coupling are derived and transient finite element method is implemented with details of the formulation given by Wei et al. [Wei and Yang (2016)]. According to the chemo-mechanical coupled constitutive relationship $\sigma_{ij} = C_{ijkl} \varepsilon_{kl} - R^* T \Delta c \delta_{ij}$ [Wei and Yang (2016)], another form for a general three-dimensional state of stress can be written as

$$\sigma_{ij} = 2\psi \varepsilon_{ij} + \lambda \varepsilon_{kk} \delta_{ij} - R^* T \Delta c \delta_{ij} \qquad (i, j = 1,2,3) \tag{17}$$

where the Lame constants $\psi = E / 2(1+\nu)$, $\lambda = E\nu / \left[(1+\nu)(1-2\nu) \right]$, $\varepsilon_{ij} \ (i, j = 1,2,3)$ are the total strain components, R^* is the universal gas constant, T is the absolute temperature, Δc is the solvent concentration change from a reference concentration, and E and ν denote elastic modulus and Poisson's ratio of the medium, respectively.

Imitating the way of thermo-mechanical coupling problem, by means of the relationship $W = \sigma_{ij} \varepsilon_{ij}^m / 2$ and $\varepsilon_{ij}^m = \varepsilon_{ij} - \alpha \Delta c \delta_{ij}$, the free energy density function W of chemo-mechanical coupling can be calculated by

$$W = \frac{1}{2}\left(2\psi\varepsilon_{ij} + \lambda\varepsilon_{kk}\delta_{ij} - R^*T\Delta c\delta_{ij}\right)\left(\varepsilon_{ij} - \alpha\Delta c\delta_{ij}\right)$$
$$= \psi\varepsilon_{ij}\varepsilon_{ij} + \frac{\lambda}{2}\left(\varepsilon_{kk}\right)^2 - R^*T\Delta c\varepsilon_{kk} + \frac{3}{2}R^*T\alpha\left(\Delta c\right)^2 \quad (i, j = 1,2,3) \tag{18}$$

where α is the chemical expansion coefficient. Focusing on a mode I crack, we have

$$\left(W_{,1}\right)_{\exp} = R^*T\left(-\varepsilon_{kk} + 3\alpha\Delta c\right)c_{,1} \tag{19}$$

Therefore, according to Eq. (16), the *J*-integral with a mode I crack can be written as

$$J_1 = \int_A \left(\sigma_{ij}u_{i,1}q_{,j} - Wq_{,1}\right)dA - \int_A R^*T\left(-\varepsilon_{kk} + 3\alpha\Delta c\right)c_{,1}qdA - \int_{A^*}\left(\mu c_{,1}\right)qdA \quad (i, j = 1,2) \tag{20}$$

In particular, it needs to be pointed out that Eq. (20) is applicable to the problem of linear elastic small deformation characterized by non-steady diffusion process for the chemo-mechanical coupled medium rather than the finite deformation problem, which is an important difference from Gao et al. [Gao and Zhou (2013)], and Bouklas et al. [Bouklas, Landis and Huang (2015)].

According to the definition of the EDI method, the *J*-integral value calculated by Eq. (20) does not depend on the size and shape of the integration domain. Typically, numerical implementations of the *J*-integral are evaluated using the isoparametric finite element method [Yildirim (2006); Dag (2007)]. An edge crack in the chemo-mechanical coupled medium is depicted for a square domain A^* with a side length of 2 *L* around the crack tip in Fig. 3.

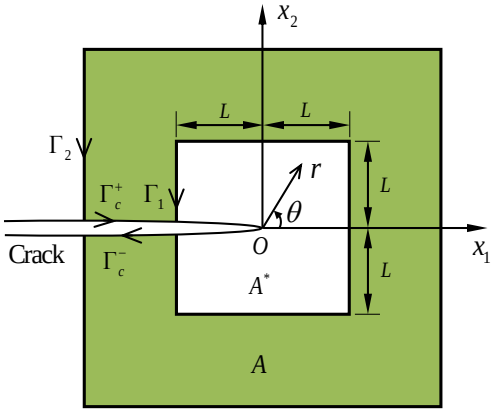

Figure 3: The equivalent domain around an edge crack tip in a chemo-mechanical coupled medium

For the purpose of the description, we define $J_1 = J_1^{\wedge} - J_{A^*}$, whereby

$$J_1^{\wedge} = \int_A \left(\sigma_{ij}u_{i,1}q_{,j} - Wq_{,1}\right)dA - \int_A R^*T\left(-\varepsilon_{kk} + 3\alpha\Delta c\right)c_{,1}qdA \tag{21}$$

$$J_{A^*} = \int_{A^*}\left(\mu c_{,1}\right)qdA \tag{22}$$

Assuming the number of isoparametric elements in the annular domain *A* is M_1 (Fig. 3),

$J_1^{\wedge}$ can be expressed as

$$J_1^{\wedge} = \sum_{s=1}^{M_1} J_1^{\wedge s} = J_1^{\wedge 1} + J_1^{\wedge 2} + \cdots\cdots + J_1^{\wedge M_1 - 1} + J_1^{\wedge M_1} \tag{23}$$

Similarly, assuming the number of isoparametric elements in square domain A^* is M_2, J_{A^*} can be written as

$$J_{A^*} = \sum_{s=1}^{M_2} J_{A^*}^{s} = J_{A^*}^{1} + J_{A^*}^{2} + \cdots\cdots + J_{A^*}^{M_2 - 1} + J_{A^*}^{M_2} \tag{24}$$

Under the case of plane condition, by using the chemo-mechanical coupled constitutive relationship $\mu = -R^*T\varepsilon_{kk} + R^*T\Delta c / c_0$ [Wei and Yang (2016)], the J-integral value calculated over one element in domain A^* and A, respectively, can be given by

$$\begin{aligned} J_1 = & \int_{-1}^{1}\int_{-1}^{1}\left(\sigma_{ij}u_{i,1}q_{,j} - Wq_{,1}\right)\left|\mathbf{J}\right|_{M_1} d\xi d\eta - \int_{-1}^{1}\int_{-1}^{1}\left[R^*T(-\varepsilon_{kk} + 3\alpha\Delta c)c_{,1}\right] q\left|\mathbf{J}\right|_{M_1} d\xi d\eta \\ & - \int_{-1}^{1}\int_{-1}^{1}\left[\left(-R^*T\varepsilon_{kk} + R^*T\,\Delta c / c_0\right)c_{,1}\right] q\left|\mathbf{J}\right|_{M_2} d\xi d\eta \qquad (i, j = 1, 2) \end{aligned} \tag{25}$$

where ξ and η are the horizontal and vertical axes of the local coordinate system, respectively. c_0 is the solvent concentration in the reference state and $\left|\mathbf{J}\right|_{M_1}$ and $\left|\mathbf{J}\right|_{M_2}$ are the determinant of the Jacobian matrix for the M_1-th and M_2-th elements, respectively.

In finite element modeling, the equivalent integral domain must be partitioned into a number of elements. Applying the Gaussian integration method, the J-integral value relative to an element can be obtained from Eq. (25). Superimposing the J-integral values for all elements covering the corresponding domain can achieve the final J-integral value.

Based on the isoparametric finite element method, the calculation procedure can be developed to evaluate the mode I J-integral under chemo-mechanical coupling.

5 Numerical examples and discussion

Numerical solutions of the mode I fracture problem considered in the present study require computation of the displacement and concentration values for the chemo-mechanical coupled medium. Thus, we have programmed a user element subroutine UEL in ABAQUS and a plane 8-node isoparametric element for chemo-mechanical coupling is developed [Wei and Yang (2016)]. The calculated displacement and concentration profiles extracted from the UEL data file are employed to evaluate the two-dimensional J-integral value in the medium.

In this section, to validate the accuracy and feasibility of the present theory and method, we firstly consider the linear elastic case with concentration-independent properties, such that the J-integral computed by the proposed procedure can be compared with those given by a purely mechanical LEFM.

Example 1

First, we take into account a rectangular linear elastic solid specimen containing a central crack subjected to normal uniaxial tension $\sigma = 30$ MPa under the two-dimensional plane

strain condition. Dimensions of the plate are shown in Fig. 4, where the height 2 *H* is 400 mm, the width 2 *W* is 200 mm, and the initial half crack length *a*=*EO*=*OG*= 20 mm with an overall crack length to width ratio of a/*W*=1:5.

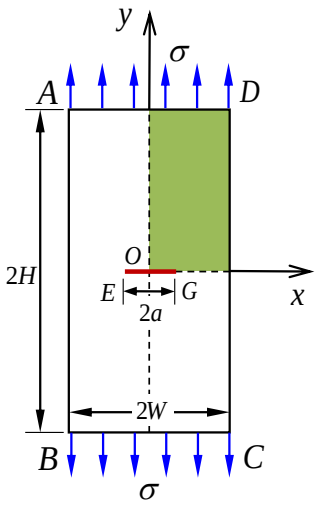

Figure 4: A rectangular solid plate with a central crack

For the present simulation, the material properties of the plate are Young's modulus $E = 200 \times 10^3$ MPa and Poisson's ratio $\nu = 0.25$. All of the above parameters were based on previously published values in the literature [Xie, Qian and Li (2009)]. An equivalent domain with plateau type *q*-function is applied to evaluate the *J*-integral value. Making use of symmetry, only a quarter of the rectangular plate is modeled using a two-dimensional finite element mesh.

The stress intensity factor [Anderson (1995)] can be written as

$$K_{\mathrm{I}} = \sigma\sqrt{\pi a}\sqrt{\sec\frac{\pi a}{2W}}\left[1 - 0.025\left(a/W\right)^2 + 0.06\left(a/W\right)^4\right] \tag{26}$$

For a homogeneous isotropic linear-elastic medium with a mode I crack, a well-known relationship for the plane strain condition is $J_1 = K_{\mathrm{I}}^2\left(1-\nu^2\right)/E$. Therefore, values can be obtained from known parameters to give K_1=243.6 $(\mathrm{MP_a}\cdot\sqrt{\mathrm{mm}})$ and J = 278.3 (N/m).

The *J*-integral value can now be calculated using the procedure developed in this example, wherein all internal and external concentrations of the medium are assumed to be zero. The calculated displacements can be input into the procedure and all chemical-related parameters set to zero such that the procedure degenerates to solve for pure mechanical fracture problem.

As shown in Fig. 5, green elements denote the annular domain A and white elements around the crack tip represent the domain *A** for evaluating the chemical integral term.

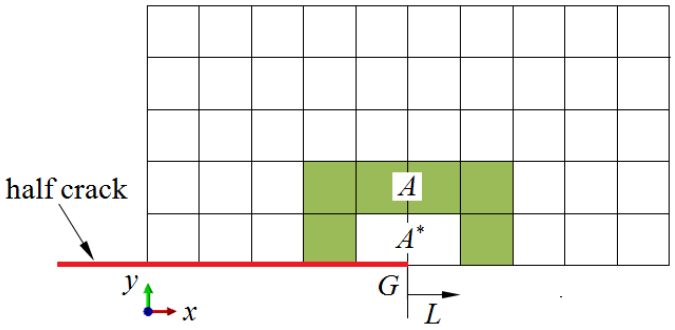

Figure 5: Equivalent integration domains around the crack tip

The size of each square is 2 mm, such that the crack tip G accurately corresponds to the number of elements. Then, the integration domain can be determined by selecting different values for L. For a quarter model in Fig. 4, when L=2 mm, there are 1×2 elements in A^* around the crack tip and when L=4 mm, A^* includes 2×4 elements around the crack tip, and so on. The domain A includes the outer elements enclosing the domain A^*.

The model consists of 5000 elements and 15301 nodes with plane 8-node isoparametric elements. Calculated values are multiplied by two and six J-integral values together with the relative error of each solution are displayed in Tab. 1.

Table 1: The influence of integration domain on the calculated values of the J-integral (N/m)

L(mm)	2	4	6	8	10	12
Elements(A^*)	1×2	2×4	3×6	4×8	5×10	6×12
J_1(present)	273.279	276.254	277.401	277.944	277.949	277.952
Error(%)	-1.804	-0.735	-0.323	-0.128	-0.126	-0.125

Under pure mechanical loading, the maximum relative error between the analytical and calculated numerical value is -1.804% for L=2 mm (Tab. 1). The error is greatest at this domain, due to the singularity at the crack tip. It is shown that when the integral domain is much closer to the crack tip, the error of numerical result of the J-integral is larger than the others. As L increases, the absolute values of numerical errors gradually decrease and when L=8 mm, 10 mm, and 12 mm, the J-integral values are approximately equal indicating good precision. The change rule of numerical results is in agreement with Xie et al. [Xie, Qian and Li (2009)], which analyzed the same solid plate and evaluated J-integral values using square elements. In addition, the similar J-integral values obtained for different domains in the present simulation confirmed the classical path-independence of the J-integral under pure mechanical loading, while ignoring the influence of the singularity at the crack tip. Importantly, the results obtained from this simulation demonstrated the accuracy of the model and by ignoring the effects of the chemical field the procedure can be used to evaluate purely mechanical problems.

Example 2

Next, the chemo-mechanical coupled fracture problem was investigated by considering an immersed rectangular specimen with a central crack in Fig. 6.

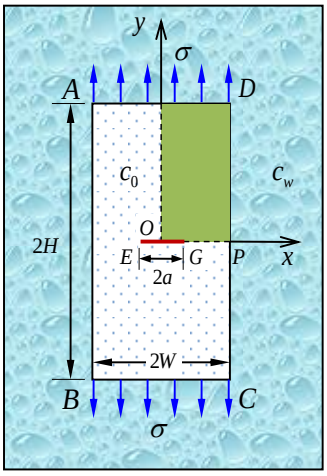

Figure 6: An immersed central cracked rectangular plate

Table 2: Material parameters of the rectangular plate

Parameter	Value
Young's modulus E	1.08 MPa
Poisson's ratio v	0.45
Diffusion coefficient D	4.9 E-10 m^2/s
Atmospheric constant R^*	8.314 J/(mol·K)
Absolute temperature T	298 K
Chemical expansion coefficient α	1.10

The dimensions of the rectangular plate are the same as the previous example (Fig. 4). The initial solvent concentration of the rectangular plate was assumed to be c_0= 200 mol/L. Simulations were conducted under the plane strain condition for two different boundary conditions: Pure mechanical loading and combined mechanical and chemical loading. Case 1 involved pure mechanical loading of $\sigma = 5\times10^{-2}$ MPa applied on the *AD* and *BC* edges and case 2 used a combined loading of $\sigma = 5\times10^{-2}$ MPa and concentration c_w=700 mol/L. All material parameters of the rectangular plate are listed in Tab. 2.

In this paper, crack edges are assumed to be traction-free and our discussion is limited to the case of an impermeable and excluded liquid-filled crack edges. Again, due to symmetry, only one quarter of the plate is modeled.

Regarding the initial conditions, Tab. 2 lists specific values for the material parameters of a rectangular plate for chemo-mechanical coupling. For the present simulation, Young's modulus E is chosen to have a value 1.08 MPa, and diffusion coefficient is taken to have a value D=4.9E-10 m^2/s originated from Luo et al. [Luo and Li (2013)]. The value of Poisson's ratio is taken as $\nu = 0.45$, and the atmospheric constant R^*=8.314 J/(mol·K) at an absolute temperature T=298 K, which is stemmed from Li et al. [Li and Mulay (2011)]. Additionally, we have chosen a value of $\alpha = 1.1$ for the chemical expansion coefficient a value which is favorable for the small deformation problem.

For a mode I crack, the y-direction stresses at the crack tip and in front of the crack tip are important parameters in researching a chemo-mechanical coupled fracture problem. Firstly, the y-direction stress field near the crack tip was investigated. If the external mechanical loading remains unchanged ($\sigma = 5\times10^{-2}$ MPa), the y-direction stress values at the crack tip decrease with the increase of the concentration because the larger concentration value can lead to the greater degree of inhomogeneous swelling in the chemo-mechanical coupled medium in Fig. 7.

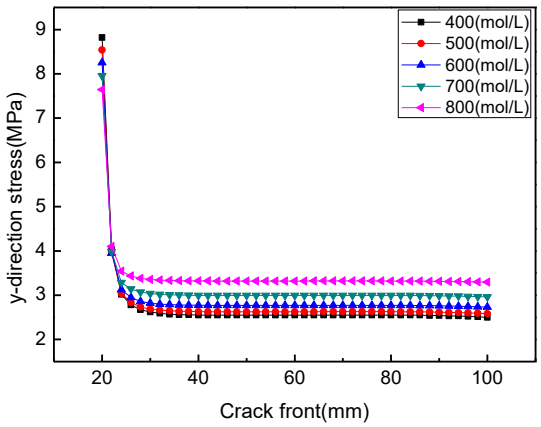

Figure 7: Variations of y-direction stress along the crack front for different concentrations at the equilibrium moment

The extent of free expansion in the y-direction on left part of the crack tip gradually increases with increasing concentration values. Consequently, stresses in the y-direction at the crack tip gradually diminish under the constant external mechanical loading ($\sigma = 5\times10^{-2}$ MPa). In other words, the effect of stress relaxation resulted from solvent redistribution gives rise to lower stress values at the equilibrium state. However, stresses at other points in front of the crack tip increase with increasing concentration values. The gradually increasing degree of expansion results in greater constraint forces in the y-direction acting in front of the crack tip, and hence the stresses are greater in this area.
When the external concentration is constant (c_w=700 mol/L), the y-direction stress values at and in front of the crack tip increase simultaneously with the increasing mechanical load, as depicted in Fig. 8.

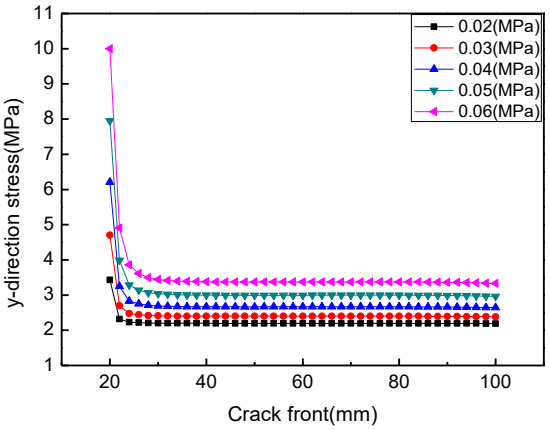

Figure 8: Variations of *y*-direction stress in front of the crack tip for different mechanical loadings

This indicates that stress values for the chemo-mechanical coupled medium are proportional to the external mechanical loading for constant concentrations.

In order to compare stress distributions near the crack tip for different boundary conditions, 50×30 elements containing the crack tip were selected for which the length of each element are 2 mm, as shown in Figs. 9(a)-9(b). The gridding mesh denotes the contour at the initial time (t=0 s).

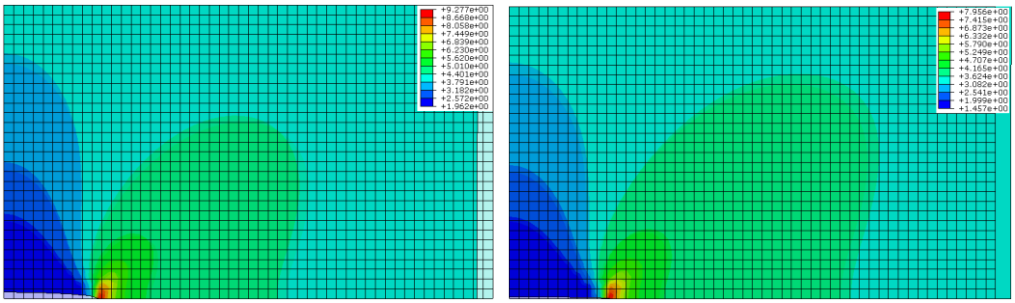

(a) Under pure mechanical loading (b) Under combined loading

Figure 9: Stress distributions in the *y*-direction around the crack tip

It was observed that in the *y*-direction, the stress distribution around the crack tip under the combined loading regime was more widespread than that under pure mechanical loading. Absorption of a large amount of solvent during the deformation phase substantially promotes solvent diffusion through the rectangular plate. However, the *y*-direction stress value at the crack tip with combined loading is less than that under pure mechanical loading, due to the effect of stress relaxation resulted from solvent redistribution at the equilibrium state. In addition, the time spent in equilibrium was much longer with combined loading than that under pure mechanical loading. The reason is that, under combined loading the rectangular plate experiences a slow deformation

process with inhomogeneous swelling.

As shown in Fig. 10, the solvent concentration outside the rectangular plate is greater than that inside the plate, and gradually spreads into the plate.

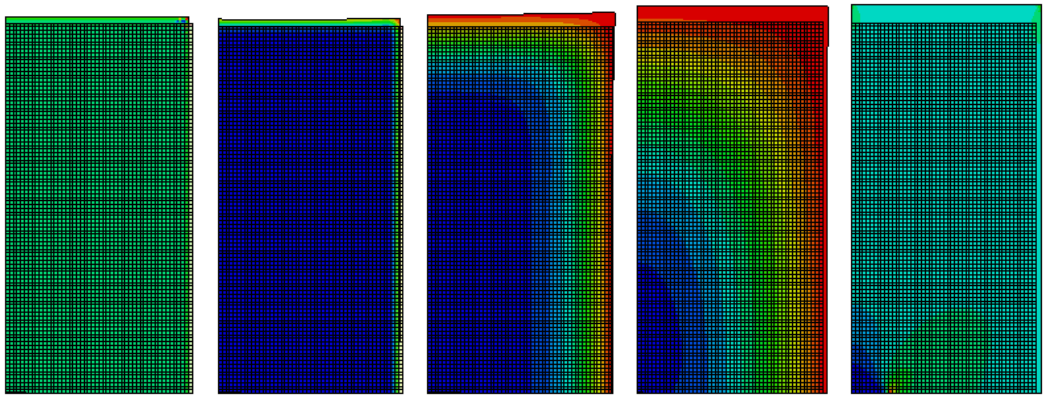

(a) t=500 s (b) t=1500 s (c) t=3100 s (d) t=4600 s (e) t=6500 s

Figure 10: Stress distributions in the *y*-direction at different time-points under combined loading

A larger concentration gradient at the initial time-point causes a faster diffusion rate, resulting in inhomogeneous swelling versus time. Consequently, the shape of the plate changes irregularly and no longer maintains a regular rectangle. In addition, an irregular sharp corner at the top right of the rectangle appeared during the deformation process. The deformation characteristics observed in this study were consistent with the literatures [Chester and Anand (2011); Zhang, Zhao, Suo et al. (2009)]. It is suggested that the top right corner is subjected to the mutual effects of the solvent around both upper and right edges at the same time. As a result, the degree of solvent absorption and the expansion rate at the top right corner are higher than what is experienced in other parts of the plate. Eventually, the entire system tends toward the equilibrium state with a smaller diffusion velocity and less inhomogeneous deformation due to a decreasing concentration gradient. Mechanical loading on the upper edge of the plate results in elongation while considerable solvent absorption leads to a volume expansion.

The *J*-integral values were calculated using six different integration domains as shown in Fig. 5. The calculated *J*-integral values under pure mechanical loading and combined loading are listed by multiplying corresponding values resulted from the procedure with 2 in Tab. 3.

From Tab. 3, similar trends were observed to those in example 1, whereby the *J*-integral values increased with *L*. Moreover, path-dependence under chemo-mechanical coupling is confirmed by the similar *J*-integral values, by neglecting the effect of the singularity at the crack tip in six domains. Moreover, the calculated *J*-integral values under combined loading are smaller than those under pure mechanical loading in the same domain. This suggests that the chemical term in Eq. (20) has a negative contribution to the *J*-integral,

and may be the result of solvent diffusion around the crack tip.

Table 3: Comparisons of the *J*-integral values for six different domains under pure mechanical loading and combined loading (N/m)

L (mm)	2	4	6	8	10	12
Elements (A*)	1×2	2×4	3×6	4×8	5×10	6×12
Mechanical loading	338.18	341.86	343.28	343.95	343.96	343.97
Combined loading	152.32	153.97	154.61	154.92	154.92	154.93

As shown in Fig. 11, when the external concentration value remains unchanged (c_w=700 mol/L), *J*-integral values are approximately equal with same external mechanical loading.

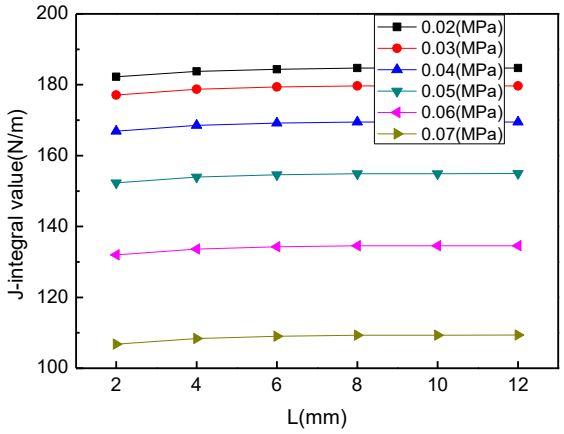

Figure 11: Variations of the *J*-integral versus domain under external mechanical loading

If the effect of the singularity at the crack tip is ignored under the same external loading in different domains, it can be demonstrated the path-independence of the *J*-integral. However, it can be observed that the *J*-integral value is smaller with larger mechanical loading in combination with the same integral domain. Moreover, there is more obvious variation in the *J*-integral value when the mechanical loading is much larger.

When the external mechanical loading is kept constant ($\sigma = 5\times10^{-2}$ MPa) the *J*-integral values are nearly equivalent with a constant concentration in different domains in Fig. 12.

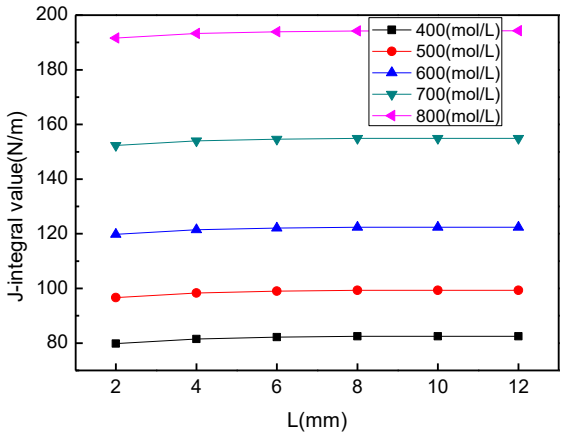

Figure 12: Variations of the *J*-integral versus domain under external concentration loading

The observed *J*-integral value increased with larger external concentration loading in the same integral domain. With greater concentrations, the extent of diffusion is much greater, resulting in a stronger coupling effect due to the chemical field. In addition, changes in the trend of the *J*-integral values were more apparent with larger concentration loading.

As mentioned above, for simplicity, L=8 mm can be chosen to calculate the *J*-integral value with sufficient accuracy. The results suggest that in the equilibrium state, the *J*-integral values decrease gradually with increasing external mechanical loading under constant concentration in Fig. 13.

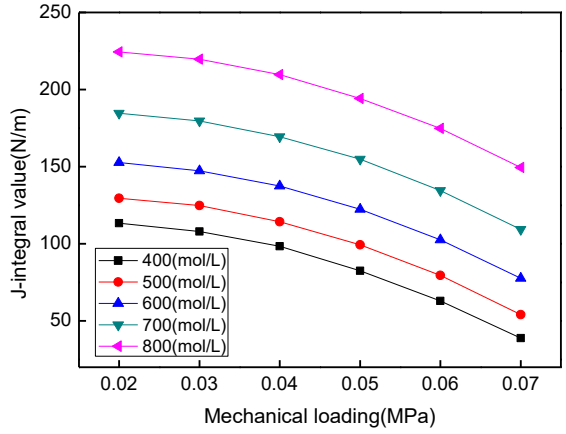

Figure 13: Variations of the *J*-integral under combined loading for different external concentrations (L=8 mm)

Furthermore, when the external mechanical loading is kept constant, the *J*-integral value increases with external concentration.

Since the *J*-integral is associated with solvent diffusion, the effect is expected to rely on

the amount of solvent within the medium. At the initial moment, the *J*-integral values become large under combined loading in Fig. 14.

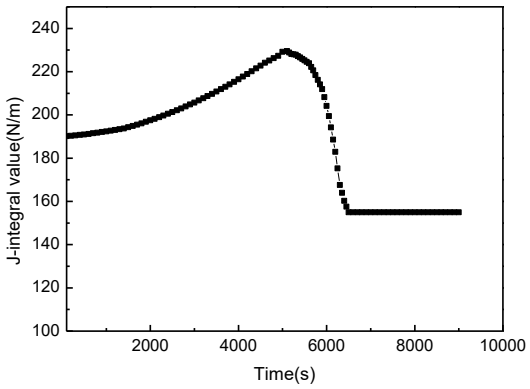

Figure 14: Variation of the *J*-integral versus time under combined loading (*L*=8 mm)

Then the *J*-integral values gradually increase to a maximum at t=5100 s and when the effect of solvent diffusion gradually reduces, the *J*-integral value becomes smaller. At equilibrium (t=6500 s), diffusion behavior tends to stop and *J*-integral value remains constant. This may be the result of solvent diffusion around the crack tip, and the solvent concentration is inhomogeneous during the diffusion phase. The change rule of *J*-integral versus time above is similar to Bouklas et al. [Bouklas, Landis and Huang (2015)].

6 Conclusion

In this paper, the *J*-integral formulation for fracture analysis and numerical implementation of a chemo-mechanical coupled medium were developed using the equivalent domain integral method. The model demonstrated path-independence for a mode I crack under chemo-mechanical coupling regarding deformation and diffusion with multi-physical mechanisms.

Based on the first law of thermodynamics, the mode I *J*-integral formulation for a chemo-mechanical coupled fracture problem was deduced. Applying the equivalent domain integral method and the chemo-mechanical coupled constitutive relationship, the mode I *J*-integral was transformed into the expression of an area integral. The accuracy of the developed procedure for evaluating the chemo-mechanical coupled mode I fracture problem was verified by comparing with the calculation values with the analytical solutions for a purely mechanical LEFM. Then, an example of a mode I fracture problem in the chemo-mechanical coupled medium was investigated and confirmed the path-independence of the *J*-integral under chemo-mechanical coupling. The effects of the integral domain, and the external chemical and mechanical loadings on the *J*-integral values were studied. The results presented the *y*-direction stress values around the crack tip under different boundary conditions and captured the variation trends of the stress field during an inhomogeneous deformation process.

The numerical procedure for calculating the chemo-mechanical coupled *J*-integral was

implemented to demonstrate the accuracy and efficiency of the path-independence of the *J*-integral, thus validating the applicability of present theoretical and numerical methods. Without the chemical field, the coupled *J*-integral becomes the conventional mechanical *J*-integral. This work provides a basic framework for analysis of the mode I fracture problem in the chemo-mechanical coupled medium. Finally, the chemo-mechanical coupled fracture problem should be investigated further combining the numerical model with experiments.

Acknowledgments: This work was supported by the National Natural Science Foundation of China under grant numbers 11472020, 11502007, 11632005, which is gratefully acknowledged.

References

Alvarez-Rivera, F.; Concheiro, A.; Alvarez-Lorenzo, C. (2018): Epalrestat-loaded silicone hydrogels as contact lenses to address diabetic-eye complications. *European Journal of Pharmaceutics and Biopharmaceutics*, vol. 122, pp. 126-136.

Anderson, T. L. (1995): *Fracture Mechanics: Fundamentals and Applications*. CRC Press, Boca Raton.

Böger, L.; Keip, M. A.; Miehe, C. (2017): Minimization and saddle-point principles for the phase-field modeling of fracture in hydrogels. *Computational Materials Science*, vol. 138, pp. 474-485.

Bonn, D.; Kellay, H.; Prochnow, M.; Ben-Djemiaa, K.; Meunier, J. (1998): Delayed fracture of an inhomogeneous soft solid. *Science*, vol. 280, no. 5361, pp. 265-267.

Bouklas, N.; Landis, C. M.; Huang, R. (2015): Effect of solvent diffusion on crack-tip fields and driving Force for fracture of hydrogels. *Journal of Applied Mechanics*, vol. 82.

Cai, S. Q.; Hu, Y. H.; Zhao, X. H.; Suo, Z. G. (2010): Poroelasticity of a covalently crosslinked alginate hydrogel under compression. *Journal of Applied Physics*, vol. 108, no. 11.

Cheng, Y.; Ren, K.; Yang, D.; Wei, J. (2018): Bilayer-type fluorescence hydrogels with intelligent response serve as temperature/pH driven soft actuators. *Sensors and Actuators B: Chemical*, vol. 255, pp. 3117-3126.

Chester, S. A.; Anand, L. (2011): A thermo-mechanically coupled theory for fluid permeation in elastomeric materials: Application to thermally responsive gels. *Journal of the Mechanics and Physics of Solids*, vol. 59, no. 10, pp. 1978-2006.

Dag, S. (2007): Mixed-mode fracture analysis of functionally graded materials under thermal stresses: A new approach using J_k-Integral. *Journal of Thermal Stresses*, vol. 30, no. 3, pp. 269-296.

Deng, K. F.; Bellmann, C.; Fu, Y. X.; Rohn, M.; Guenther, M. et al. (2018): Miniaturized force-compensated hydrogel-based pH sensors. *Sensors and Actuators B: Chemical*, vol. 255, pp. 3495-3504.

Ding, S. H.; Liu, Q. N. (2018): a multi-layered model for heat conduction analysis of thermoelectric material strip. *Computer Modeling in Engineering & Sciences*, vol. 114,

no. 3, pp. 335-349.

Gao, Y. F.; Zhou, M. (2013): Coupled mechano-diffusional driving forces for fracture in electrode materials. *Journal of Power Sources*, vol. 230, pp. 176-193.

Guo, F. N.; Guo, L. C.; Yu, H. J.; Zhang, L. (2014): Thermal fracture analysis of nonhomogeneous piezoelectric materials using an interaction energy integral method. *International Journal of Solids and Structures*, vol. 51, pp. 910-921.

Haftbaradaran, H.; Qu, J. M. (2014): A path-independent integral for fracture of solids under combined electrochemical and mechanical loadings. *Journal of the Mechanics and Physics of Solids*, vol. 71, pp. 1-14.

Hui, C. Y.; Long, R.; Ning, J. (2013): Stress relaxation near the tip of a stationary mode I crack in a poroelastic solid. *Journal of Applied Mechanics*, vol. 80, no. 2.

Javanbakht, S.; Namazi, H. (2018): Doxorubicin loaded carboxymethyl cellulose/graphene quantum dot nanocomposite hydrogel films as a potential anticancer drug delivery system. *Materials Science and Engineering: C*, vol. 87, pp. 50-59.

Khorasani, M. T.; Joorabloo, A.; Moghaddam, A.; Shamsi, H.; Mansoori Moghadam, Z. (2018): Incorporation of ZnO nanoparticles into heparinised polyvinyl alcohol/chitosan hydrogels for wound dressing application. *International Journal of Biological Macromolecules*, vol. 114, pp. 1203-1215.

Kim, J. H.; Paulino, G. H. (2002): Finite element evaluation of mixed mode stress intensity factors in functionally graded materials. *International Journal for Numerical Methods in Engineering*, vol. 53, no. 8, pp. 1903-1935.

Kim, J. H.; Paulino, G. H. (2003): Mixed-mode *J*-integral formulation and implementation using graded elements for fracture analysis of nonhomogeneous orthotropic materials. *Mechanics of Materials*, vol. 35, no. 1-2, pp. 107-128.

Kuna, M. (2006): Fem-techniques for thermo-electro-mechanical crack analyses in smart structures. *Solid Mechanics and Its Applications*, vol. 127, pp. 131-143.

Lei, J.; Wang, H. Y.; Zhang, C. Z.; Bui, T. Q.; Garcia-Sanchez, F. (2014): Comparison of several BEM-based approaches in evaluating crack-tip field intensity factors in piezoelectric materials. *International Journal of Fracture*, vol. 189, pp. 111-120.

Li, H.; Mulay, S. S. (2011): 2D simulation of the deformation of pH-sensitive hydrogel by novel strong-form meshless random differential quadrature method. *Computational Mechanics*, vol. 48, pp. 729-753.

Li, F. Z.; Shih, C. F.; Needleman, A. (1985): A comparison of methods for calculating energy release rates. *Engineering Fracture Mechanics*, vol. 21, no. 2, pp. 405-421.

Li, X. (1993): *J*-Integral and *J**-Integral in thermal stress conditions. *Engineering Fracture Mechanics*, vol. 45, pp. 713-715.

Luo, R. M.; Li, H. (2013): Parameter study of glucose-sensitive hydrogel: Effect of immobilized glucose oxidase on diffusion and deformation. *Soft Materials*, vol. 11, pp. 69-74.

Ma, L. H.; Yang, Q. S. (2018): Micromechanics-based elastic fields of closed-cell

porous media. *Computer Modeling in Engineering & Sciences*, vol. 114, no. 2, pp. 239-259.

Mahinroosta, M.; Farsangi, Z. J.; Allahverdi, A.; Shakoori, Z. (2018): Hydrogels as intelligent materials: A brief review of synthesis, properties and applications. *Materialstoday Chemistry*, vol. 8, pp. 42-55.

Mao, Y. W.; Anand, L. (2018): A theory for fracture of polymeric gels. *Journal of the Mechanics and Physics of Solids*, vol. 115, pp. 30-53.

Moura, B.; Shih, C. F. (1987): A treatment of crack tip contour integrals. *International Journal of Fracture*, vol. 35, pp. 295-310.

Nikishkov, G. P.; Atluri, S. N. (1987): An equivalent domain integral method for computing crack-tip integral parameters in non-elastic, thermo-mechanical fracture. *Engineering Fracture Mechanics*, vol. 26, pp. 851-867.

Noselli, G.; Lucantonio, A.; Mcmeeking, R. M.; DeSimone, A. (2016): Poroelastic toughening in polymer gels: A theoretical and numerical study. *Journal of the Mechanics and Physics of Solids*, vol. 94, pp. 33-46.

Park, J. S.; Choi, Y. H.; Kim, J.; Im, S. (2015): Energy release rate in the presence of residual and thermal stresses. *International Journal of Solids and Structures*, vol. 59, pp. 73-78.

Pizzocolo, F.; Huyghe, J. M.; Ito, K. (2013): Mode I crack propagation in hydrogels is step wise. *Engineering Fracture Mechanics*, vol. 97, pp. 72-79.

Raju, I. S.; Shivakumar, K. N. (1990): An equivalent domain integral method in the two-dimensional analysis of mixed mode crack problems. *Engineering Fracture Mechanics*, vol. 37, pp. 707-725.

Rice, J. R.; Cleary, M. P. (1976): Some basic stress diffusion solutions for fluid-saturated elastic porous media with compressible constituents. *Reviews of Geophysics and Space Physics*, vol. 14, no. 2, pp. 227-241.

Ricoeur, A.; Kuna, M. (2008): The thermoelectromechanical *J*-integral and thermal permeability of cracks. *Key Engineering Materials*, vol. 385-387, pp. 569-572.

Ricoeur, A.; Kuna, M. (2009): Electrostatic tractions at dielectric interfaces and their implication for crack boundary conditions. *Mechanics Research Communications*, vol. 36, no. 3, pp. 330-335.

Shao, Y.; Jia, H. Y.; Cao, T. Y.; Liu, D. S. (2017): Supramolecular hydrogels based on DNA self-assembly. *Accounts of Chemical Research*, vol. 50, no. 4, pp. 659-668.

Shih, C. F.; Moran, B.; Nakamura, T. (1986): Energy release rate along a three-dimensional crack front in a thermally stressed body. *International Journal of Fracture*, vol. 30, pp. 79-102.

Shivakumar, K. N.; Raju, I. S. (1992): An equivalent domain integral method for three-dimensional mixed-mode fracture problem. *Engineering Fracture Mechanics*, vol. 42, pp. 935-959.

Sun, J. Y.; Zhao, X. H.; Illeperuma, W. R.; Chaudhuri, O.; Oh, K. H. et al. (2012): Highly stretchable and tough hydrogels. *Nature*, vol. 489, pp. 133-136.

Tang, J. D.; Li, J. Y.; Vlassak, J. J.; Suo, Z. G. (2017): Fatigue fracture of hydrogels. *Extreme Mechanics Letters*, vol. 10, pp. 24-31.

Walters, M. C.; Paulino, G. H.; Dodds, R. H. (2004): Stress-intensity factors for surface cracks in functionally graded materials under mode-I thermomechanical loading. *International Journal of Solids and Structures*, vol. 41, pp. 1081-1118.

Wang, X.; Hong, W. (2012): Delayed fracture in gels. *Soft Matter*, vol. 8, no. 31, pp. 8171-8178.

Wei, W.; Yang, Q. S. (2016): A finite element procedure for analysis of chemo-mechanical coupling behavior of hydrogels. *Computer Modeling in Engineering & Sciences*, vol. 112, no. 1, pp. 33-58.

Wilson, W. K.; Yu, I. W. (1979): The use of the *J*-integral in thermal stress crack problems. *International Journal of Fracture*, vol. 15, no. 4, pp. 377-387.

Xie, D.; Qian, Q.; Li, C. A. (2009): *Numerical Calculation Method and Engineering Application in Fracture Mechanics*. Science Press, Beijing (in Chinese).

Yang, C. H.; Lin, Y. Y. (2018): Time-dependent fracture of mode-I cracks in poroviscoelastic media. *European Journal of Mechanics-A/Solids*, vol. 69, pp. 78-87.

Yang, F.; Wang, J.; Chen, D. P. (2006): The energy release rate for hygrothermal coupling elastic materials. *Acta Mechanica Sinica*, vol. 22, no. 1, pp. 28-33.

Yildirim, B. (2006): An equivalent domain integral method for fracture analysis of functionally graded materials under thermal stresses. *Journal of Thermal Stresses*, vol. 29, no. 4, pp. 371-397.

Yu, P. F.; Chen, J. Y.; Wang, H. L.; Liang, X.; Shen, S. P. (2018): Path-independent integrals in electrochemomechanical systems with flexoelectricity. *International Journal of Solids and Structures*, pp. 1-9.

Yu, P. F.; Wang, H. L.; Chen, J. Y.; Shen, S. P. (2017): Conservation laws and path-independent integrals in mechanical-diffusion-electrochemical reaction coupling system. *Journal of the Mechanics and Physics of Solids*, vol. 104, pp. 57-70.

Yu, H. J.; Wu, L. Z.; Guo, L. C.; Ma, J. W.; Li, H. (2012): A domain-independent interaction integral for fracture analysis of nonhomogeneous piezoelectric materials. *International Journal of Solids and Structures*, vol. 49, pp. 3301-3315.

Zhang, J. P.; Zhao, X. H.; Suo, Z. G.; Jiang, H. Q. (2009): A finite element method for transient analysis of concurrent large deformation and mass transport in gels. *Journal of Applied Physics*, vol. 105, no. 9.

Zhang, M.; Qu, J. M.; Rice, J. R. (2017): Path independent integrals in equilibrium electro-chemo-elasticity. *Journal of the Mechanics and Physics of Solids*, vol. 107, pp. 525-541.